Journal of Physics: Conference Series

PAPER • OPEN ACCESS

An evaluation of different measurement strategies to measure wind turbine near wake flow with small multicopter UAS

To cite this article: N Wildmann and J Kistner 2024 *J. Phys.: Conf. Ser.* **2767** 042004

View the article online for updates and enhancements.

You may also like

- Bubbles versus biofilms: a novel method for the removal of marine biofilms attached on antifouling coatings using an ultrasonically activated water stream
M Salta, L R Goodes, B J Maas et al.
- Landscape-scale characterization of Arctic tundra vegetation composition, structure, and function with a multi-sensor unoccupied aerial system
Dedi Yang, Bailey D Morrison, Wouter Hantson et al.
- Onboard device for UAS remote identification
D S Bragin, D R Urazayev, A A Konev et al.

The Electrochemical Society
Advancing solid state & electrochemical science & technology

DISCOVER
how sustainability intersects with electrochemistry & solid state science research

This content was downloaded from IP address 129.247.247.240 on 17/06/2024 at 12:33

Journal of Physics: Conference Series **2767** (2024) 042004 doi:10.1088/1742-6596/2767/4/042004

An evaluation of different measurement strategies to measure wind turbine near wake flow with small multicopter UAS

N Wildmann[1] **and J Kistner**[1]

[1] Deutsches Zentrum für Luft- und Raumfahrt e.V., Institut für Physik der Atmosphäre, Oberpfaffenhofen, Germany

E-mail: norman.wildmann@dlr.de

Abstract. Wind turbine wake flow, especially in the near wake, that is up to one rotor diameter D downstream, is subject to interaction between tip vortices and ambient turbulence. These interactions are important to understand wake decay, but most difficult to measure with common instrumentation. Small uncrewed aerial systems (UAS) can help to measure at such locations where no masts can be installed. We contrast two measurement strategies, the hover flight with multiple UAS and cross-section flights with single UAS. We show that both strategies have advantages; the cross-section flights provide a full picture of the width and wind speed deficit across the rotor diameter whereas multi-UAS hover flights can provide more reliable turbulence intensity and turbulent flux measurements at specific locations. With both strategies, tip vortices can be detected and qualified to characterize the state of wake decay at different positions. A fit to the vortex models Lamb-Oseen and Burnham-Hallock allows to estimate circulation and core radius of the vortices. For best characterization of the wake, we recommend to combine the hover and cross-section flight strategies in future.

1. Introduction

Uncrewed aerial systems (UAS) have been increasingly utilized for wind energy research in the past decade to provide in situ validation data of flow in the wake of wind turbines [1, 2, 3, 4]. Especially the use of small multicopters is compelling for their ease of use, low cost and the data quality that can be achieved. In the field of atmospheric measurements, particularly wind measurements, multicopter UAS can be a flexible tool to measure at locations which are usually difficult to reach with in situ instrumentation. One such location is the near wake of a wind turbine. Within the near wake and in the transition to the far wake, complex physics are involved in the break-down of tip vortices and mixing of air from the free flow into the wake which define the persistence of the wake. Remote sensing instrumentation such as Doppler wind lidar can only reveal parts of the physics, due to the inherent limitations in spatial and temporal resolution. With lidar, only wind components along the line-of-sight can be measured directly, and the volume averaging and temporal resolution depend strongly on the specific instrument and measurement strategy [5, 6]. Multicopter UAS have the advantage that in situ three-dimensional measurements can be performed at most flexible locations and even temperature, humidity and pressure information can be obtained if appropriate sensors are carried. Nevertheless, limitations of UAS are in the measurement duration, the spatial coverage

Content from this work may be used under the terms of the Creative Commons Attribution 4.0 licence. Any further distribution of this work must maintain attribution to the author(s) and the title of the work, journal citation and DOI.
Published under licence by IOP Publishing Ltd

and the resolution of very small scales. For the systems as they were operated in this study, we are limited to 15 minute flight time, spatial coverage of few hundred meters and a resolution of 2 Hz which means that eddies of 5 m size can be resolved at 10 m s^{-1} mean wind speed [7, 8]. Those limitations also depend on the deployed system and measurement strategy. In this study we look at two different strategies to measure the flow inside a wind turbine wake, either by multi-point stationary measurement with a fleet of UAS or by trajectory flights of single drones. Thielicke et al. (2021) [3] as well as Li et al. (2022) [9] showed how the wake can be scanned with single UAS in trajectory flight mode. We contrast both principle strategies with measurements in close succession in the near wake of a wind turbine in complex terrain. Wetz and Wildmann (2023) [4] showed how a fleet of five drones can be used to obtain spatial information of the flow in the wake, including turbulence intensity and momentum fluxes. They did not use external sensors attached to the drones, but calculated wind from avionic data. They found that turbulence in the near wake is very much defined by tip vortices and wake meandering. In this study we look at measurements with exactly that fleet of UAS during the same series of experiments and focus in on the tip vortices. Section 2 describes the experiment and measurement setup, Sect. 3 presents results of mean wind speed deficit, tip vortex measurements and momentum fluxes in the near wake.

2. Methods

2.1. Experiment description

Measurements were carried out in the vicinity of an Enercon E-82 wind turbine in complex terrain. The wind turbine has a rotor diameter of $D = 82$ m and a hub height of $z_h = 138$ m. Experiments at the site were carried out on six days throughout the year 2022 [4]. In a neutral and almost stationary boundary-layer on 7 November 2022, four successive flights were performed with the UAS fleet within 80 minutes. The first two flights were done with five UAS simultaneously according to the strategy described in Wetz and Wildmann (2023) [4] at hub height z_h. The last two flights were performed with three UAS, one was collecting inflow data 2 D upstream, the other two were flying four cross-sections per flight downstream of the wind turbine in 0.5 D and 1 D respectively at a constant flight speed of 1 m s^{-1} and at an altitude of $z = 120$ m. The altitude had to be set lower than z_h due to the legal constraints that flights further than 1 D from the obstacle are limited to 120 m above ground level. Figure 1 shows a sketch of the measurement configuration. The dots in Fig 1b show the hover positions, and the lines the cross-section flights in two distances. Since a misalignment between wind direction and turbine yaw angle was observed frequently and wind direction was changing rapidly within $\pm 10°$, the measured wake (red shade in Fig. 1) can differ from the projected wake (blue shade) that was used to define the measurement points. Table 1 gives a list of the four flights that are in the focus of this analyses. The first two flights are following the established *hover* flight strategy, the latter two are flights with cross-section horizontal profiling (*cross*). In the first flight, UAS #15 could not fly due to technical reasons. In flight #1 and #2, UAS#11 is flying at $y = 1$ D outside the wake to obtain a reference wind speed. In flight #3 and #4, UAS #22 is profiling at $x = -2D$ upstream to obtain the reference simultaneously to the wake measurements. Wind speed U, wind direction Ψ and potential temperature θ from those reference flights are shown in Fig. 2. It can be seen that relatively small shear and veer and almost no gradient in potential temperature is observed on average, but a high variability between each profile is present.

2.2. Wind and turbulence estimation

Measuring the three-dimensional wind with the SWUF-3D fleet is only based on avionics data of the autopilot without an external sensor. The drone is the sensor. We use the wind retrieval as described in Wildmann et al. (2022) [10] which yield the final equation for the wind vector

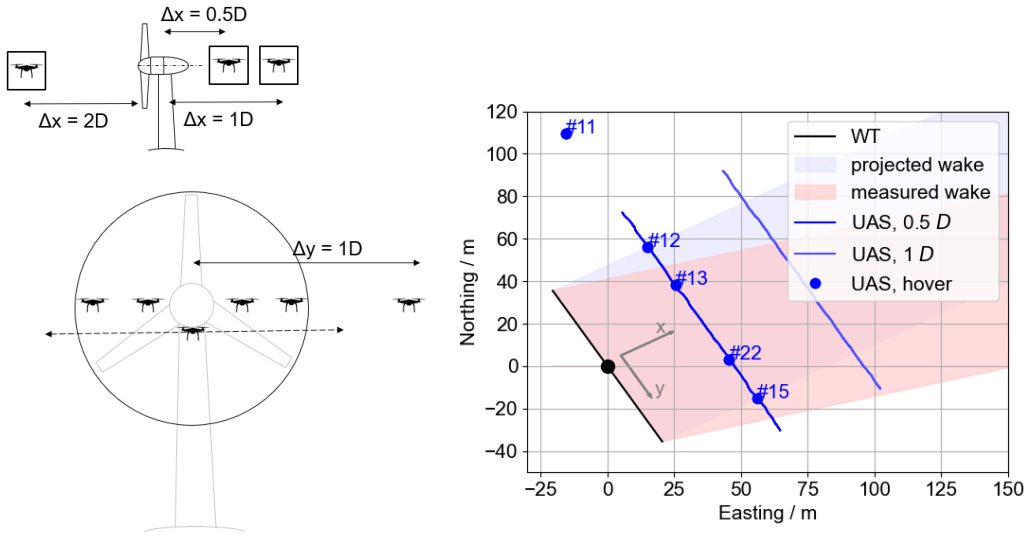

Figure 1. a) Sketch of the measurement configuration of the UAS fleet in the vicinity of a wind turbine. b) Plan view of the measurement layout.

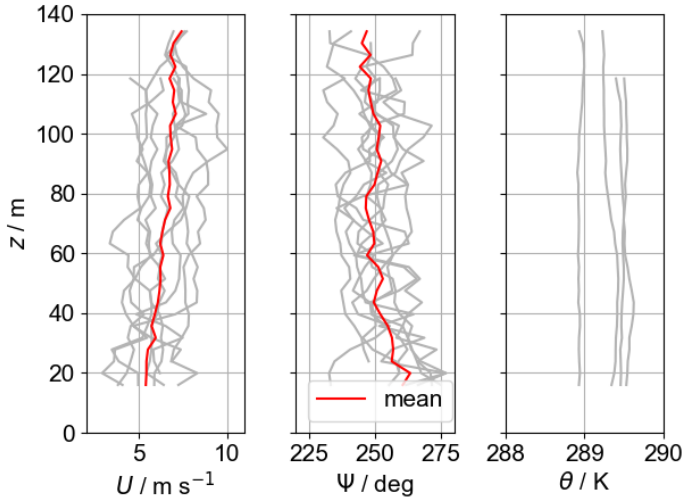

Figure 2. Vertical profiles up to hub height outside the wake between 10:12 UTC and 11:30 UTC. The mean of all profiles is shown in red. For θ, only ascents are used.

Table 1. Measurement flights on 7 November 2022 and meteorological conditions

#	t UTC	UAS	pattern	Ψ deg	U m s^{-1}	TI %	T °C	RH %	$\frac{\Delta\theta}{\delta z}$ K m^{-1}
1	10:12	11, 12, 13, 22	hover	245	7.8	15	9.7	75	0.1
2	10:39	11, 12, 13, 15, 22	hover	249	7.7	18	9.9	73	-0.1
3	11:02	11, 12, 22	cross	256	7	21	10	70	-0.2
4	11:19	11, 12, 22	cross	253	7	12	10.1	69	-0

in the geodetic coordinate system:

$$\begin{pmatrix} u_g \\ v_g \\ w_g \end{pmatrix} = \mathbf{R}(\varphi, \theta, \psi) \begin{pmatrix} u_b \\ v_b \\ w_b \end{pmatrix} - \begin{pmatrix} v_x \\ v_y \\ v_z \end{pmatrix} \quad , \tag{1}$$

where φ, θ and ψ are the roll, pitch and yaw angles of the quadrotor which compose the rotation matrix R that is used to rotate the calibrated wind speeds from the body frame (u_b, v_b, w_b) into the geodetic frame. The linear velocities v_x, v_y and v_z are especially important for wind measurements in forward flight to translate the true airspeed measurement of the quadrotor to the wind speed. Figure 3 shows an illustration of the coordinate systems.

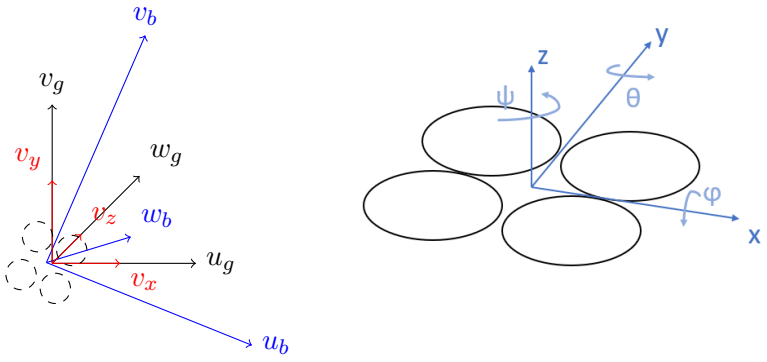

Figure 3. Coordinate systems for wind calculation are shown on the left. Blue is the airspeed vector in body-frame coordinates, black the wind vector in geodetic coordinates and red the translational velocity vector of the UAS. The quadrotor UAS is sketched with dashed circles. On the right, the body-fixed coordinate system of the UAS is shown with the rotation angles associated to the axes.

In default processing, the wind vector in the geodetic frame is transformed into the meteorological coordinate system with u the zonal, v the meridional wind component and positive w pointing upwards. In our case we rotate those components into a wind turbine-fixed coordinate system with u the streamwise velocity component, v the spanwise wind component and w as in the meteorological frame, pointing upwards. The variables are used according to this definition in the following. The linear velocity is a product of the flight controller's internal Kalman filter that fuses GPS velocity with inertial measurement unit (IMU) data. Compared to the hover state validation in the field [11, 7] and in the wind tunnel [8], the linear velocity is one additional source of uncertainty. Typical GPS velocity uncertainty estimates are below 0.2 m s^{-1}. The covariance estimate of the Kalman filter is even one order of magnitude smaller, so that using the specified GPS velocity uncertainty is a conservative estimate. Propagating this uncertainty and the estimated uncertainties of the wind tunnel verification experiments of $\sigma_u < 0.3$ m s^{-1} for the wind speed range we are facing, we yield an overall uncertainty of $\sigma_u < 0.36$ m s^{-1} and thus only a small increase in uncertainty through forward flight if the flight velocity is small compared to the wind velocity and a small angle of sideslip ($< 20°$) can be guaranteed.
Turbulence intensity is calculated with $I = \frac{\sigma_U}{\overline{U}}$ and added turbulence in the wake with $\Delta I = \sqrt{I^2 - I_0^2}$, where I_0 is the inflow turbulence intensity [4].

2.3. Barometric pressure and height

For analyses of wake dynamics and identifying vortices, it is interesting to look at the pressure difference in the wake. The autopilot which is used as the flight controller in the SWUF-3D

fleet features a barometric pressure sensor with a resolution of 1.2 Pa and can thus be used to measure small differences in pressure. The sensor is used by the flight controller to control the altitude so that in a heterogeneous pressure field, the drone will change the altitude relative to the ground in order to maintain constant pressure. GPS is used in an extended Kalman filter to correct barometer drift on longer time scales and very rapid changes in pressure on the sub-second scale will not be considered by the controller due to a low pass filter. This means that rapid pressure changes as in tip vortices can be detected in the pressure readings and changes of pressure on a medium time scale of a few seconds to minutes will be visible in the altitude readings by the GPS.

2.4. Wake vortex models

For comparison of tip vortex measurements and estimation of their circulation Γ and core radius r_c, we use two models that describe the tangential velocity in dependency of the radius $V_t(r)$. First, a Lamb-Oseen model as described in Holzäpfel et al. (2000) [12]:

$$V_t(r) = \frac{\Gamma_0}{2\pi r}\left(1 - \exp\frac{-1.26r^2}{r_c^2}\right) \quad , \tag{2}$$

and second the well-known Burnham-Hallock model [13]:

$$V_t(r) = \frac{\Gamma_0}{2\pi r}\frac{r^2}{r^2 + r_c^2} \quad . \tag{3}$$

3. Results

3.1. Wind measurements in forward flight

In a different study, Alexa (2024) [14] showed that forward flight measurements at a low flight velocity of $v_x = 1$ m s^{-1} do not show systematic biases compared to short hover periods along the flight path. In our study, hover periods were only included for short 10-s periods at the ends of the cross-section legs of the flight. At these locations and also comparing the two flight directions, no systematic error can be detected. It thus appears that at the used slow forward flight speed, accurate wind measurements can be obtained without an external sensor attached to the UAS.

3.2. Wind speed deficit

Figure 4 shows the results of averaged wind component measurements in the wake for the four regarded flights. The ambient conditions including stability and TI are given in Table 1. The lines show flights #3 and #4. The asterisks show 12-minute averaged wind speeds for flights #1 and #2 with four drones in the wake. For the streamwise velocity, a normalization by the inflow velocity u_∞ is done. It shows that there is a good agreement between forward flight and hover flights with a slightly higher wind speed deficit for hover flights which can be attributed to the different flight altitudes.

The wind speed deficit in the wind turbine wake, which can best be observed in the streamwise component, has two local maxima at 0.5 D close to the rotor tips (minima in the solid lines in Fig. 4a), but it is almost flat at the 1 D distance downstream. This shows that for the neutrally stratified atmosphere in that case, vortex structures quickly break down and wake recovery sets in. These findings are in line with a previous study [4] that showed the same pattern with more measurements at the same site.

The hover flights additionally reveal that the variance of wind measurements is higher at the outer parts of the wake, close to the projected rotor tips. Strong peaks in the v-component in the time series of UAS hovering in the outer parts of the wake are indicating the presence of remaining vortex structures in 0.5 D downstream the turbine and cause the increased variability. This will be examined in more detail within the next section.

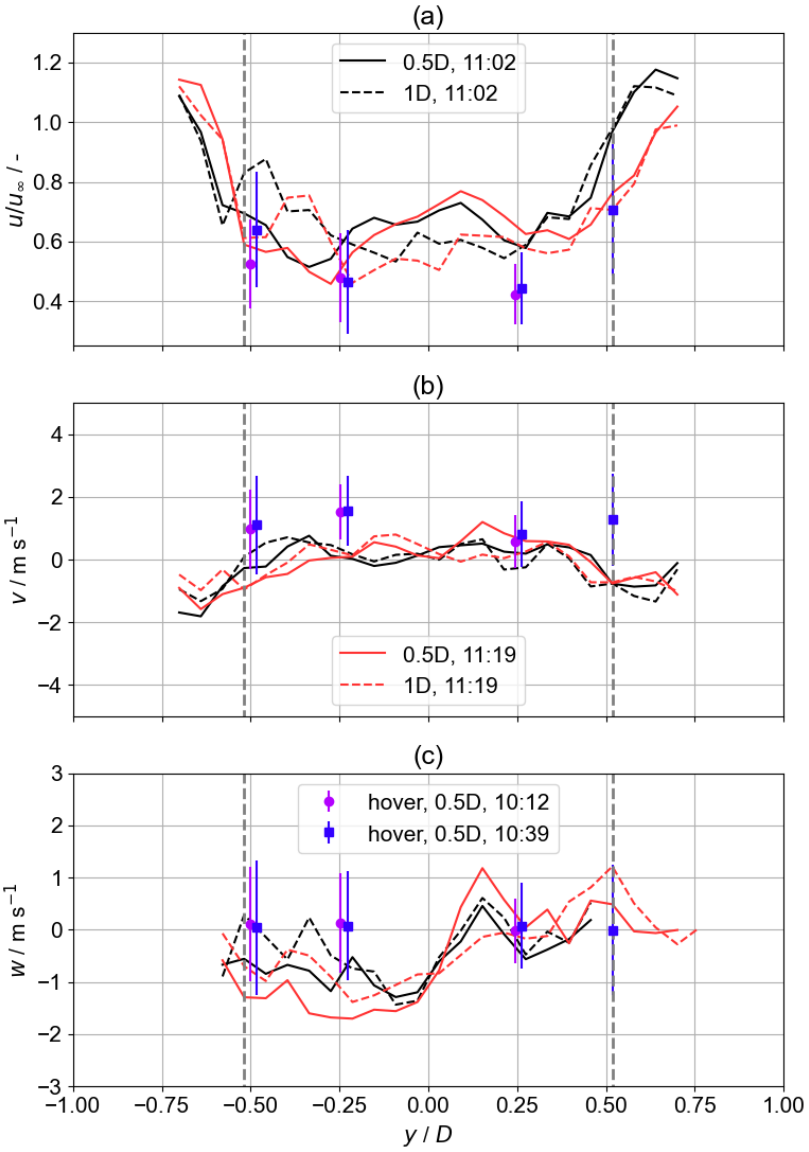

Figure 4. u-,v- and w-component of the wind vector as measured with the UAS fleet for all flights downstream. Streamwise velocity is normalized by the inflow velocity estimate u_∞. Dashed lines are in $1D$ distance and solid lines in $0.5D$. Red vs. black lines are two separate flights. The hover flight results are shown in blue dots with standard deviations. Grey dashed lines visualize the rotor tips locations.

3.3. Wake tip vortices

The decay of wind turbine wakes is based on the breakup of tip vortices in the ambient turbulence and further downstream mixing of air into the low wind-speed region. Identifying vortices with in situ measurements is particularly challenging because of their complex dynamics and three-dimensional structure. With the two methods we present here, the hover flight at fixed points and the cross-section forward flight, we have two ways to measure the temporal and spatial extent of the vortices, respectively. Although, strictly speaking, both methods are spatio-temporal measurements, because the vortex develops even in the short time of the UAS passing through

and the hover flight is never perfectly at the same position in the highly dynamic wake vortex system. The advection velocity of the vortex is close to the inflow velocity and thus much larger than the flight velocity of the drone. Due to that, the measurement during the cross flight is quite similar to a measurement at a fixed position. Mauz et al. (2019) [2] measured wake vortices with a fixed-wing aircraft. With the faster flying aircraft, a measurement that is closer to a spatial snapshot can be achieved, but with a lower resolution.
Figure 5a shows measurements at the edge of the wake, i.e. at a distance of -0.73...-0.48 D in y-direction from the center of the turbine as measured in a single leg of the cross-section flight. Figure 5b gives time series of the hover flight measurements at both sides of the turbine at 0.5 D distance in y-direction. In both types of measurements, signatures of wake vortices can be seen in the u- and v-component of the wind, but also in the barometric pressure p and even in the vertical velocity component w. It is important to notice that measurements of vertical wind with a magnitude of $w > 5$ m s^{-1} and at $U > 8$ m s^{-1} are out of the calibration range and subject to large uncertainties and were removed from the dataset. The two cases that are shown illustrate that for both strategies it is possible that multiple vortices are measured in close succession, which shows in multiple successive peaks in the velocity components. In other parts of the flights, single vortices can also appear, predominantly for the cross-section flight, depending on where the vortices moved within the meandering frame of the wake during the flight.
Figure 6 further shows a closer view on single vortices. The inset sketches in the plots indicate how the vortex moves with the mean wind speed (in x-direction) through the flight path (relative to the airflow) of the drone. From the relative amplitude of u- and v-component, it can be determined where the drone hits the vortex. If the u-component is larger, as in (a) and (b), the drone passed outside the core radius, if u is smaller, as in (c) it must be inside. The sign of the u-component ((a) negative vs. (b) and (c) positive) shows on which side of the vortex the measurements were taken. The change of sign in the v-component determines the rotational direction. Naturally, vortices measured on the other side of the wind turbine nacelle rotate in the other direction (as can be seen in Fig. 5b for the v-components). The red curve in the figures shows a fit of the Lamb-Oseen vortex model, which fits better than the Burnham-Hallock (blue) for the same combination of $\Gamma = 40$ m^2 s$^-1$ and $r_c = 0.6$ m. The light red curves shows cross-sections of the Lamb-Oseen model vortex at y =0...1 m. Misaka et al. (2015) [15] showed for aircraft wake vortices that the best-fitting model depends on the vortex age and roll-up. A younger vortex will show a better fit with Lamb-Oseen compared to the Burnham-Hallock model. Our measurements show that the same applies to wind turbine tip vortices. The determined circulation and core radius can only be a rough estimate. As the significant vertical wind component w in the measurement shows, the vortices are not perfectly two-dimensional at the location where they are measured with the drone and the radius is relatively small compared to the drone size, so that it is uncertain if the drone can resolve the vortex in its actual magnitude. However, Mauz et. al (2019) [2] calculated comparable values for a slightly larger wind turbine theoretically and from fixed-wing UAS measurements, so that the measurements can be considered realistic.

3.4. Turbulence and momentum fluxes

One kind of calculation that can only be done from stationary measurements in the hover flight pattern is the retrieval of momentum fluxes with the eddy-covariance method. Wetz and Wildmann (2023) [4] presented horizontal momentum fluxes in the wake and showed how they change sign and transport energy from high wind speed to low wind speed regions. We now also include vertical momentum fluxes in Fig. 7a where possible for the two flights that are regarded in this study. Unfortunately, at the hover positions where the tip vortices are observed and outside of the wake, the wind speeds are at levels that are out of the calibration range

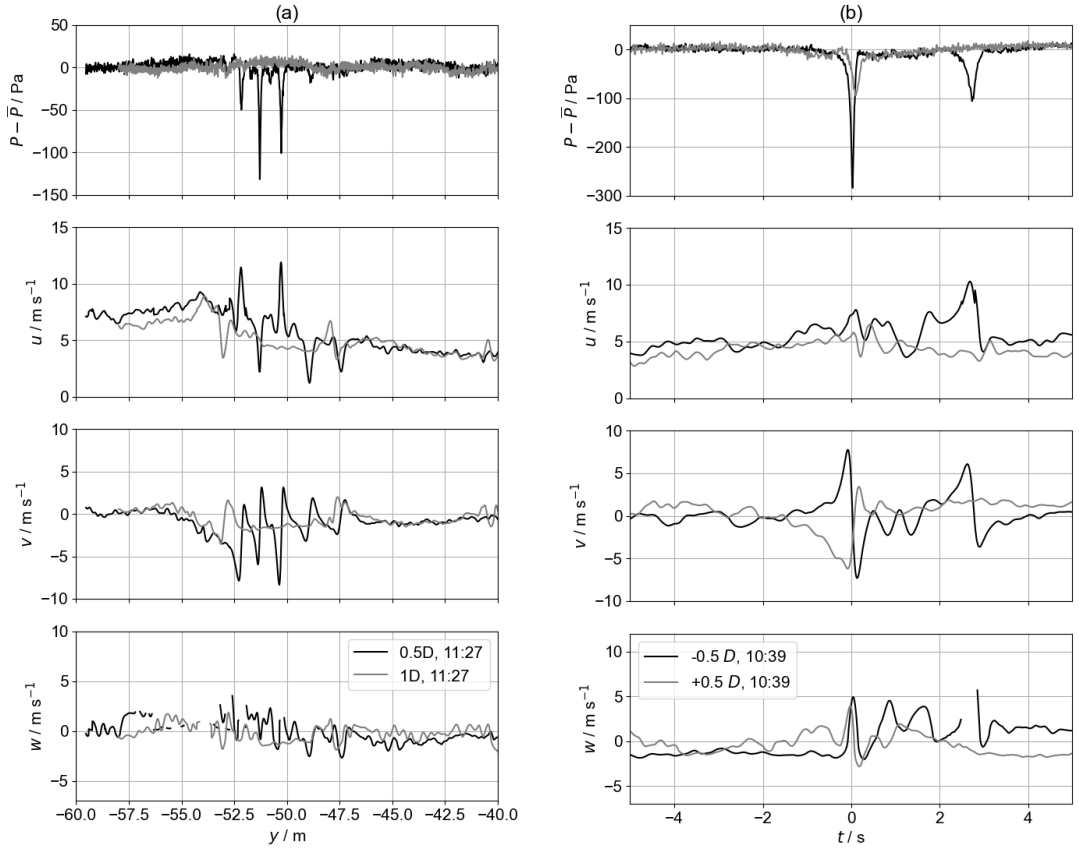

Figure 5. Space-series of cross-section flight #4 (a) and time series of hover flight #2 (b) for the variables pressure $p - \overline{p}$ and the three wind components u, v and w showing the passing of wake vortices.

for the vertical velocity measurements and the values are therefor cross-contaminated by the horizontal wind. Only the values inside the wake can thus be shown for $\overline{u'w'}$ and $\overline{v'w'}$. The horizontal flux $\overline{u'v'}$ behaves as described in [4], changing the sign twice towards the center of the wake, because of the higher wind speeds in the center at $x = 0.5\ D$. The vertical fluxes show a consistent picture between the two hover flights, but for drawing conclusions about the physics in the wake, not enough data points are available. The uncertainty in both plots is shown with error bars and is set to the values that were determined in Wildmann and Wetz (2022) [10]. Figure 7b shows the added turbulence intensity ΔI from hover flights (blue and purple dots) and also an estimate from the cross-flights. The cross-flight values are running averages with a moving window of 20 m width. With such small windows, not all scales of turbulence are included in the average. This leads to smaller values of I compared to the hover flights and therefor even negative values of ΔI, since hover flights are used for the estimation of I in the inflow. They do however allow to see that for the resolved scales, turbulence is highest at the rotor tips at both downstream distances $y = 0.5..1\ D$. The high values at the outer part of the wake are partly due to tip vortices and wake meandering. They are more pronounced at the closer downstream distance ($0.5\ D$).

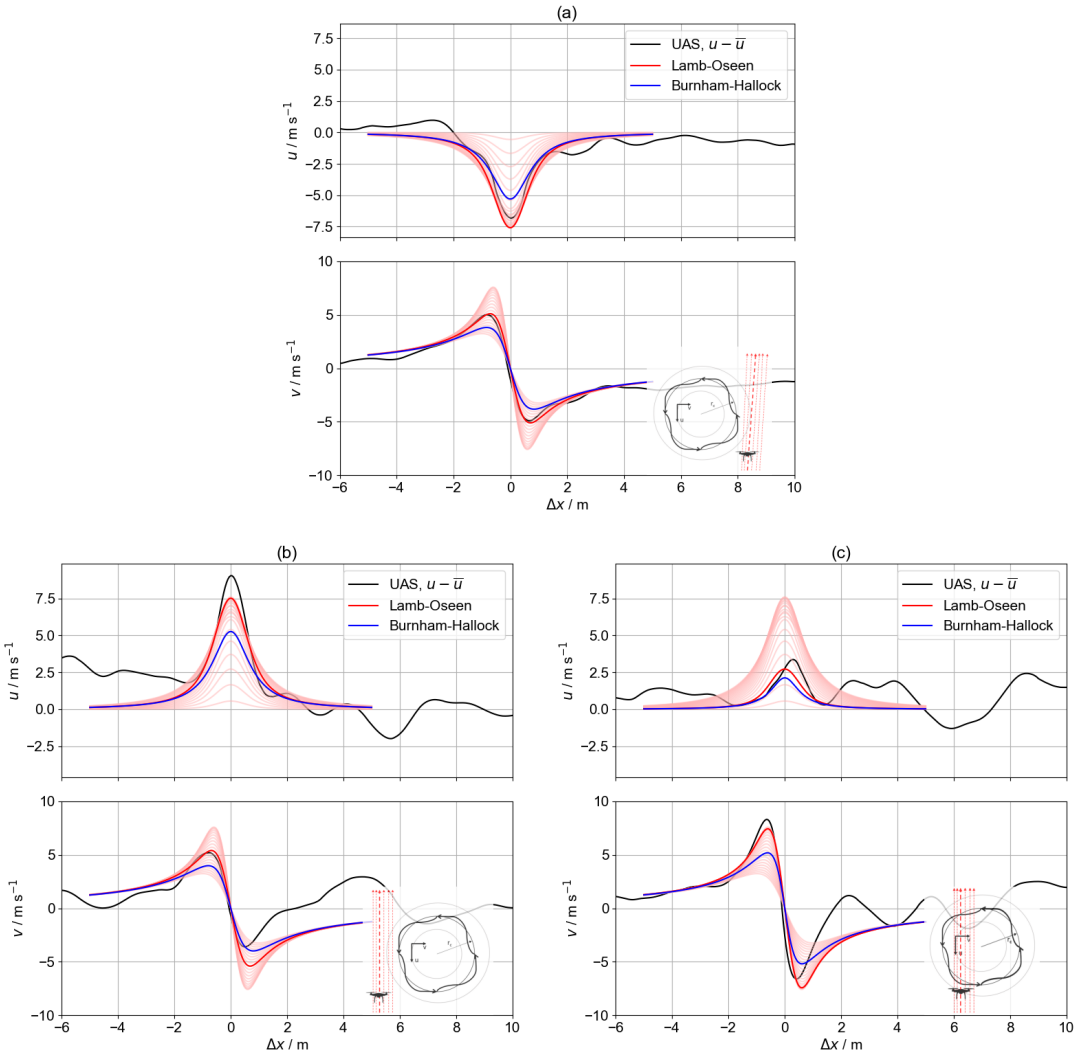

Figure 6. Close-up of single wake vortex measurements for the cross-section flight (a) and two cases of hover flight #2. (b and c). The streamwise u and lateral v component are shown over the travel distance of the vortex relative to the drone Δx. The red and the blue thick lines show a fitted Lamb-Oseen and Burnham-Hallock vortex cross-section, respectively. Light red lines are shifted cross-sections of the Lamb-Oseen model for $y = 0 \ldots 1$ m. The image on the bottom right shows the location where the vortex passes the drone presumably.

4. Conclusions

UAS-based measurements are a new possibility to obtain in-situ observations at locations where it was not easily feasible before. The near-wake of an operating wind turbine is one such location. This study shows that different flight strategies can provide different pieces of information about the wake. While cross-section flights can provide highly resolved spatial measurements of the wind speed deficit, hovering systems at multiple points allow to derive turbulence statistics at those locations more accurately. We present turbulence intensity and momentum fluxes as examples which are particularly interesting to characterize the mixing of air in the wake. Tip vortices in the near wake of a wind turbine can be measured with both strategies, but careful analyses are necessary to derive vortex parameters. The wake flow in the flights that we

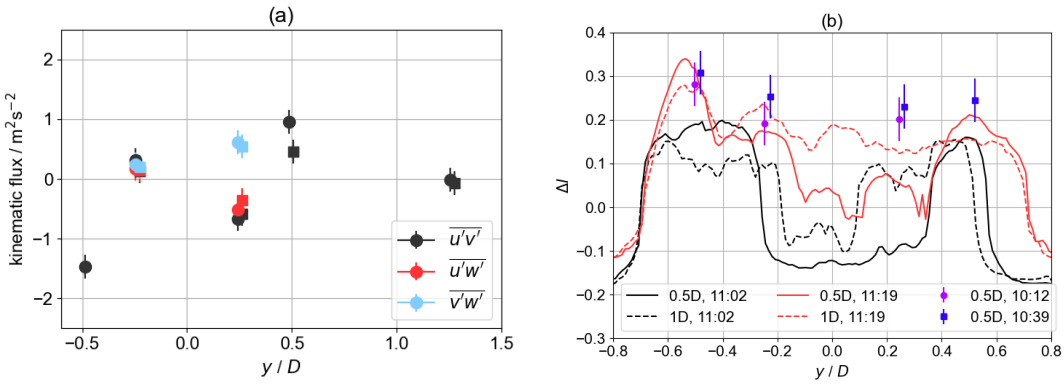

Figure 7. The three components of the Reynolds stress tensor $\overline{u'v'}$,$\overline{u'w'}$ and $\overline{v'w'}$ for flights #1 and #2. Error bars show the uncertainty $\sigma_f = 0.2$ m^2 s^{-2}. Circles (rectangles) are for the flight at 10:12 UTC (10:39 UTC).

presented was highly non-stationary and subject to strong turbulence. It also showed the three-dimensional flow in the wake often went outside of the calibration range for vertical velocity of the UAS. Further validation and calibration of the w-component especially at horizontal wind speeds $U > 8$ m s^{-1} is necessary in future to increase confidence in tip vortex measurements. Repeating similar measurements in a stable boundary layer is recommended for the future to obtain more fundamental information about near-wake flow and tip vortex breakdown. In November 2023, first measurements at the WiValdi research park in Northern Germany have already been done with up to ten drones simultaneously to obtain more measurement points for reliable turbulence statistics inside the wake. The number of measurement points and the number of flights shall be further increased in the near future.
We conclude that both strategies, hover and cross-section flights with multicopter UAS appear to be complementary and in a future effort, they should be combined to get a full picture of wake dynamics.

Acknowledgements

This research has been supported by the HORIZON EUROPE European Research Council (grant no. 101040823, ESTABLIS-UAS). Special thanks goes to EnBW and in particular Carolin Schmitt for allowing measurements in close vicinity to their WT and for providing the WT data.

References

[1] Wildmann N, Hofsäß M, Weimer F, Joos A and Bange J 2014 *Adv. Sci. Res.* **11** 55–61
[2] Mauz M, Rautenberg A, Platis A, Cormier M and Bange J 2019 *Wind Energy Science* **4** 451–463
[3] Thielicke W, Hübert W, Müller U, Eggert M and Wilhelm P 2021 *Atm. Meas. Tech.* **14** 1303–1318
[4] Wetz T and Wildmann N 2023 *Wind Energy Science* **8** 515–534
[5] Wildmann N, Vasiljevic N and Gerz T 2018 *Atm. Meas. Tech.* **11** 3801–3814
[6] Letizia et al 2023 *Front. in Mech. Eng.* **9** ISSN 2297-3079
[7] Wetz T and Wildmann N 2022 *Journal of Physics: Conference Series* **2265** 022086
[8] Kistner J, Neuhaus L and Wildmann N 2024 *EGUsphere* **2024** 1–28
[9] Li Z, Pu O, Pan Y, Huang B, Zhao Z and Wu H 2022 *Sust. E. Tech. and Ass.* **53** 102537 ISSN 2213-1388
[10] Wildmann N and Wetz T 2022 *Atm. Meas. Tech.* **15** 5465–5477
[11] Wetz T, Wildmann N and Beyrich F 2021 *Atm. Meas. Tech.* **14** 3795–3814
[12] Holzäpfel F, Gerz T, Frech M and Dörnbrack A 2000 *Journal of Aircraft* **37** 1001–1007
[13] Burnham D C and Hallock J N 1982 *US. Dept. of Transp. Fed. Av. Adm., Tech Report* **4** 590–599
[14] Alexa A 2023 MSc Thesis University of Innsbruck
[15] Misaka et al *7th AIAA Atm. and Space Env. Conf.* chap 3023, p 10